

Book of Abstracts RETURN Dissemination Workshop

*Original*

Book of Abstracts RETURN Dissemination Workshop / Costamagna, Elisa; Mazzoglio, Paola. - ELETTRONICO. - (2024), pp. 1-343. (Intervento presentato al convegno RETURN Dissemination Workshop tenutosi a Torino (IT) nel 1-2 February 2024) [10.5281/zenodo.10598007].

*Availability:*

This version is available at: 11583/2985677 since: 2024-02-05T11:49:34Z

*Publisher:*

*Published*

DOI:10.5281/zenodo.10598007

*Terms of use:*

This article is made available under terms and conditions as specified in the corresponding bibliographic description in the repository

*Publisher copyright*

(Article begins on next page)

**Exact thermodynamics of an extended Hubbard model of single and paired carriers in competition**

Fabrizio Dolcini\* and Arianna Montorsi†

*Dipartimento di Fisica and Unità INFN, Politecnico di Torino, I-10129 Torino, Italy*

(Received 11 October 2001; published 27 March 2002)

By exploiting the technique of Sutherland's species, introduced in Phys. Rev. B **63**, 121103, we derive the exact spectrum and partition function of a one-dimensional extended Hubbard model. The model describes a competition between dynamics of single carriers and short-radius pairs, as a function of on-site Coulomb repulsion ( $U$ ) and filling ( $\rho$ ). We provide the temperature dependence of the chemical potential, compressibility, local magnetic moment, and specific heat. In particular the latter turns out to exhibit two peaks, both related to "charge" degrees of freedom. Their origin and behavior are analyzed in terms of kinetic and potential energy, both across the metal-insulator transition point and in the strong-coupling regime.

DOI: 10.1103/PhysRevB.65.155105

PACS number(s): 71.10.Fd, 71.27.+a, 71.30.+h, 05.30.-d

**I. INTRODUCTION**

In condensed matter, electron systems in regimes of high correlation are known to be suitably modeled by the Hubbard Hamiltonian<sup>2</sup> and its generalizations.<sup>3-9</sup> For such models, the finite-temperature properties are the ultimate results which theoretical investigations (numerical or analytical) aim to reach, in view of comparisons to experimental data. Indeed some observables exhibit intriguing features as a function of the temperature, which deserve an accurate interpretation.

In particular, the thermodynamics of the standard Hubbard model has been widely investigated. In  $D=1$  this was done by different exact approaches: in Refs. 10 and 11 and in Ref. 12 for the usual case of nearest-neighbor hopping, while in Ref. 13 for the case of long-range hopping. In dimensions greater than 1 recent results were obtained by exact diagonalization on small clusters<sup>14,15</sup> and numerical investigations,<sup>16,17</sup> whereas the case  $D=\infty$  has been examined in Ref. 18 by iterated perturbation theory.

All the results show interesting behaviors as a function of temperature, with varying the filling and the Coulomb repulsion. This is the case, for instance, for the specific heat, where a double-peak structure as well as the appearance of quasiuniversal crossing points were found, which features were already noticed in some experimental data.<sup>19,20</sup> In the strong-coupling regime the presence of a two-peak structure is usually related to the so-called "spin" and "charge" degrees of freedom. Numerical results in one<sup>11</sup> and two dimensions<sup>16,17</sup> show that, at least at half-filling, such structure survives also at moderate couplings.

Contrary to the ordinary Hubbard model, which has been approached through several techniques, for the extended Hubbard models most finite-temperature results have been carried out by means of mean-field theories.<sup>7</sup> In one dimension, however, it is known that traditional approaches to many-body systems such as mean-field or Fermi-liquid theories are either unreliable or inapplicable. As a consequence, both numerical techniques (like the density matrix renormalization group<sup>21</sup>) and nonconventional analytical approaches (like bosonization<sup>22</sup>) have to be supported by comparison with exact solutions, whenever available; this is basically the

reason for the growing interest devoted to finite-temperature *exact* results.

The main technique within exact approaches to one-dimensional (1D) systems is the Bethe ansatz (BA), either in the coordinate<sup>23</sup> or in the algebraic<sup>24</sup> formulation. Such technique amounts to guessing for a given model eigenstates of the form proposed by Bethe,<sup>25</sup> and in particular it has been extensively applied to models of correlated electrons; for instance, the BA equations for a wide class of integrable extended Hubbard models<sup>26</sup> have been recently derived in Ref. 27. However, the actual solution of these equations, i.e., the evaluation of the quantum numbers characterizing the system (quasi momenta), is in general quite difficult, and some hypothesis on their distribution (string hypothesis<sup>28</sup>) has typically to be conjectured. In order to derive the complete solution and calculate thermodynamic quantities, one is thus reduced to solving a system of infinitely many coupled integral equations, which requires dramatic numerical effort. More recently, considerable progress has been achieved through the alternative approach of the quantum transfer matrix,<sup>29</sup> which yields dealing with only a finite number of coupled integral equations. This has been done for the ordinary Hubbard model<sup>12</sup> and for the  $t$ - $J$  model,<sup>30</sup> as well as for an extended Hubbard model with bond-charge interaction.<sup>31</sup>

Nevertheless, determining the actual properties of a model at finite temperature for arbitrary parameter values remains in general a very hard task, even when the model is proved to be integrable and its ground-state features are possibly derived.

In the present paper we present the exact thermodynamics of a one-dimensional extended Hubbard Hamiltonian (described in Sec. II) whose exact analytical ground-state properties were obtained in Ref. 1 by a technique different from the BA. We called that technique the Sutherland species (SS) technique, and here we show how it can be exploited to derive explicitly the whole spectrum and the partition function of the model (Sec. III). In Sec. IV we calculate some thermodynamic quantities: namely, the chemical potential, the compressibility, the local magnetic moment, and the specific heat. In particular in Sec. IV D we focus on the specific heat, which turns out to exhibit a two-peaks structure. The origin of such structure and the differences with respect to the standard Hubbard model are discussed in Sec. V.

## II. MODEL

The Hamiltonian we are interested in reads

$$\hat{\mathcal{H}} = -t \sum_{\langle i,j \rangle, \sigma} (1 - \hat{n}_{i-\sigma}) c_{i\sigma}^\dagger c_{j\sigma} (1 - \hat{n}_{j-\sigma}) + Y \sum_{\langle i,j \rangle} c_{i\uparrow}^\dagger c_{i\downarrow}^\dagger c_{j\downarrow} c_{j\uparrow} + U \sum_i \hat{n}_{i\uparrow} \hat{n}_{i\downarrow}. \quad (1)$$

Here  $c_{i\sigma}^\dagger, c_{i\sigma}$  are fermionic creation and annihilation operators on a one-dimensional chain with  $L$  sites,  $\sigma \in \{\uparrow, \downarrow\}$  is the spin label,  $\hat{n}_{j\sigma} = c_{j\sigma}^\dagger c_{j\sigma}$ , and  $\langle i, j \rangle$  stands for neighboring sites. The Fock space  $\mathbb{F}$  of the system is the product of the  $L$  four-dimensional vector spaces  $V_j$  related to each site  $j$ ; each  $V_j$  is spanned by the basis  $|\uparrow\rangle_j, |\downarrow\rangle_j, |0\rangle_j, |\downarrow\uparrow\rangle_j$ , which we shall also denote in the following as  $|e_\alpha\rangle_j$ ,  $\alpha = 1, \dots, 4$ , respectively. We shall adopt for the 1D lattice *open* boundary conditions; as usual, these are not expected to affect the results in the thermodynamic limit.

In the Hamiltonian (1) the three terms (which will also be denoted as  $\mathcal{H}_t$ ,  $\mathcal{H}_Y$ , and  $\mathcal{H}_U$ ) represent, respectively, the kinetics of single carriers, the kinetics of paired carriers, and the on-site Coulomb repulsion.

More explicitly,  $\mathcal{H}_t$  describes the hopping of single electrons towards empty sites. This term is thus reminiscent of the so-called “ $U = \infty$  Hubbard model.” An important difference must be however highlighted: the latter model reads  $\mathcal{P} \sum_{\langle i,j \rangle, \sigma} c_{i\sigma}^\dagger c_{j\sigma} \mathcal{P}$ , where  $\mathcal{P} = \prod_i (1 - \hat{n}_{i\uparrow} \hat{n}_{i\downarrow})$  projects the doubly occupied sites out of the Hilbert space (which in that case is actually  $3^L$  dimensional); in contrast, the term  $\mathcal{H}_t$  in Eq. (1), although not involving pairs, does not exclude their presence in the state of the system.<sup>32</sup>

The second term in Eq. (1) is in contrast a kinetic term of pairs only; it is worth stressing that the model deals with pairs having a very short radius; in fact, while in models such as BCS one has several pairs within a radius of the coherence length, here the radius of a pair is thought of as small with respect to the lattice constant and is actually taken as zero. This kind of term is also used in the so-called Penson-Kolb-Hubbard model (see Ref. 8), where one investigates the effects of the pair dynamics without explicitly entering the microscopic mechanism yielding their formation.<sup>33</sup> We also point out that the first and second terms in Eq. (1), though describing the kinetic of different kind of carriers (single and pair, respectively), *do not* commute at all.

The third term is traditionally the most important term for Hubbard-like models; indeed, according to Hubbard’s picture, it is the parameter that should drive the metal-insulator transition in the  $d$ -transition-metal compounds. Loosely speaking, the ratio  $U/t$  can be thought as proportional to the inverse of the pressure applied on the sample: by increasing the pressure one reduces the lattice spacing and thus makes the hopping amplitude more relevant with respect to  $U$ .

The first two terms of the Hamiltonian are in general competing: indeed  $\mathcal{H}_t$  would favor delocalized waves of single carriers, avoiding the formation of pairs;  $\mathcal{H}_Y$  lowers instead the energy when electrons form tightly bound pairs moving along the chain. This competition is in addition modulated by

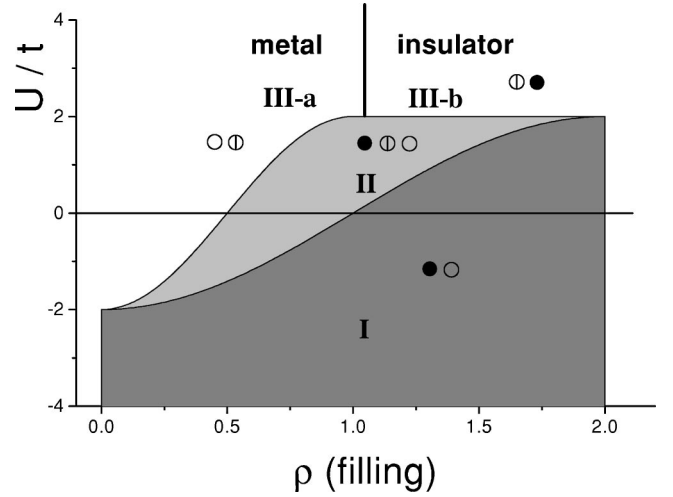


FIG. 1. Ground-state phase diagram of the model (1) for  $Y = -t$ , from Ref. 1. Open, barred, and solid circles, respectively, represent empty, singly occupied, and doubly occupied sites in the ground state.

both the term in  $U$  and the filling, i.e., the density  $\rho$  of electrons in the chain. This can be seen by examining the case

$$Y = -t. \quad (2)$$

Indeed for this value of the coupling constant the model has been proved to be integrable<sup>26</sup> and the exact ground-state phase diagram (reported in Fig. 1) has been obtained in Ref. 1. Tuning  $U$  and  $\rho$  the model exhibits interesting features; for instance, even when the value of filling is  $\rho < 1$  and at moderate ( $U < 2t$ ) Coulomb repulsion, it is energetically favorable for the system to form pairs and let them move instead of having only singly occupied sites.

In region I the ground state (g.s.) is made of only doubly occupied and empty sites; in region II we have also singly occupied sites (either  $|\uparrow\rangle$  or  $|\downarrow\rangle$ ). In region III-a the g.s. is that of the  $U = \infty$  Hubbard model and is made of singly occupied sites (metal). In region III-b the g.s. of the model reduces to that of the atomic limit of the Hubbard model (insulator). At half-filling ( $\rho = 1$ ) a charge gap  $\Delta_c = U - 2t$  opens for any  $U \geq 2t$ .

We wish to stress that, unlike many exactly solved electron systems, the model (1) is not particle-hole invariant: indeed the first term breaks up the invariance; this leads to the shape of the phase diagram shown in Fig. 1, which is asymmetrical with respect to half-filling.

## III. SPECTRUM OF THE SYSTEM

In the following we shall assume  $Y = -t$ , since such a relation allows for the integrability, as observed above. In this case, the Hamiltonian (1) can be rewritten in the form

$$\hat{\mathcal{H}} = \sum_{\langle i,j \rangle} \hat{T}_{i,j} + U \sum_i \hat{n}_{i\uparrow} \hat{n}_{i\downarrow}, \quad (3)$$

where  $\hat{T}_{i,j}$  accounts for the first two interaction terms in Eq. (1). The term in  $U$  is easily checked to commute with  $\sum_{\langle i,j \rangle} \hat{T}_{i,j}$ . Due to the condition (2),  $\hat{T}_{i,j}$ , exhibits the structure of a *generalized* off-diagonal permutator between physical species (PS), which are the local vectors  $|e_\alpha\rangle$ 's. More explicitly, while the ordinary off-diagonal permutator, when acting on  $|e_\alpha\rangle_j \otimes |e_\beta\rangle_{j+1}$ , returns  $|e_\beta\rangle_j \otimes |e_\alpha\rangle_{j+1}$  for any  $\alpha \neq \beta$  and zero for  $\alpha = \beta$ , a generalized one makes the exchange or gives zero according to the specific values of  $\alpha$  and  $\beta$ . In our case,  $\hat{T}_{i,j}$  permutes the PS of two neighboring sites only if one belongs to group  $A$  and the other to group  $B$ , where

$$A = |\uparrow\rangle, |\downarrow\rangle, |\downarrow\uparrow\rangle, \quad B = |0\rangle. \quad (4)$$

In all the remaining cases  $\hat{T}_{i,j}$  gives zero. The above groups  $A$  and  $B$  of PS can be identified with the Sutherland species of the model (1) (see Ref. 1); the notion of SS is strictly related to the structure of the Hamiltonian and not to that of the underlying Hilbert space.<sup>34</sup> In  $D=1$  a generalized permutator between PS has the same eigenvalues as an ordinary permutator between the corresponding SS. This is actually what allows us to provide the exact spectrum, as we shall see below.

The Fock space  $F$  of the system is  $F = \bigoplus_{N=0}^{2L} H_N$ , where  $H_N$  is the  $N$ -electron Hilbert space ( $\hat{N} = \sum_{i=1}^L \hat{n}_{i\uparrow} + \hat{n}_{i\downarrow}$ ). However, due to the properties of the Hamiltonian, it turns out to be useful to rearrange  $F$  in terms of  $H_{N_A}$ , i.e., the spaces spanned by all vectors that have a definite number  $N_A$  of sites occupied by states of species  $A$  ("A sites" henceforth). Clearly  $N_B = L - N_A$ . According to the properties of the generalized permutator fulfilled by  $\mathcal{H}$ , the latter commutes with  $\hat{N}_A = \sum_{i=1}^L \hat{n}_{i\uparrow} + \hat{n}_{i\downarrow} - \hat{n}_{i\uparrow} \hat{n}_{i\downarrow}$ , and thus  $H_{N_A}$  is preserved by the dynamics (this would hold in any dimension). In addition, dealing with an open chain, one can have  $3^{N_A}$  possible sequences  $\mathcal{S}$  of  $A$  sites for a fixed number  $N_A$ . Notice also that, since (i) the first term of Eq. (3) only permutes  $A$  with  $B$  and gives zero otherwise and (ii) the second term merely counts the number of doubly occupied sites, also the sequence  $\mathcal{S}$  is preserved by the dynamics, and it can be identified with an invariant subspace within  $H_{N_A}$ . The dimension of each of these  $3^{N_A}$  subspaces is  $\binom{L}{N_A}$ , accounting for all possible actual positions of  $A$  sites along the chain. One can repeat the above foliation for all  $H_{N_A}$ 's ( $N_A$  runs from 0 to  $L$ ) and check that the Fock space is completely recovered:

$$\sum_{N_A=0}^L 3^{N_A} \binom{L}{N_A} = 4^L, \quad (5)$$

so that  $F = \bigoplus_{N_A=0}^L H_{N_A}$ .

Focusing on a given  $H_{N_A}$ , one can characterize each of its basis vector by specifying two discrete-valued functions  $S(m)$  and  $J(m)$  ( $m = 1, \dots, N_A$ ). The former, which is valued 1 (for  $|\uparrow\rangle$ ), 2 (for  $|\downarrow\rangle$ ), or 3 (for  $|\downarrow\uparrow\rangle$ ), determines the sequence  $\mathcal{S}$  of  $A$  sites and, thus, the invariant subspace in which the vector lies; the latter, which is valued 1 to  $L$ ,

determines the actual positions of the  $m$ th  $A$  site along the chain. The basis vectors can therefore be referred to as  $|\{\mathcal{S}\}, \{\mathcal{J}\}\rangle$ , where " $\{\}$ " is to remind one that  $\mathcal{S}$  and  $\mathcal{J}$  are functions.

In realizing that the Hamiltonian can be separately diagonalized within each subspace characterized by a given  $A$  sequence  $\mathcal{S}$ , it is also crucial to observe that each such invariant subspace can be put in a one-to-one correspondence with the states of  $N_A$  spinless fermion space (or equivalently with the states of  $N_A$  spin-1/2 model with magnetization  $L - N_A$ ) as follows:

$$|\{\mathcal{S}\}, \{\mathcal{J}\}\rangle \leftrightarrow \left( \prod_{m=1}^{N_A} a_{J(m)}^\dagger \right) |0\rangle, \quad (6)$$

where  $a^\dagger$  are the creation operators for a spinless fermions and  $\{\mathcal{S}\}$  the sequence of the subspace.

Similarly to what has been done in Ref. 6 for another extended Hubbard model, it is also easy to derive the form of an effective Hamiltonian for the spinless fermion states: indeed, since the first term in Eq. (3) reduces to a permutator between SS, it actually acts on the considered subspace in the same way as a free Hamiltonian  $-t \sum_{\langle i,j \rangle} a_i^\dagger a_j$  acts on the spinless problem space. The second term simply counts the number of species  $A$  of kind  $|\downarrow\uparrow\rangle$ , namely,  $N_{\downarrow\uparrow} = \sum_{i=1}^L n_{i\uparrow} n_{i\downarrow} \equiv N - N_A$ . Therefore the spectrum in each subspace is given by

$$E(\{n_k^A\}; N) = \sum_{k=1}^L (-2t \cos k - U) n_k^A + UN, \quad (7)$$

where  $\{n_k^A\}$  are quantum numbers valued 0 or 1,  $k = \pi l / (L + 1)$  ( $l = 1, \dots, L$ ), and  $N$  is the total number of electrons (which ranges from  $N_A$  to  $2N_A$ ). The eigenvectors are given by the antitransform through Eq. (6) of spinless fermion eigenstates  $[\prod_k \sum_{i=1}^L \sin(ki) a_i^\dagger] |0\rangle$ , where the product is over  $N_A$  of the  $L$  allowed values of  $k$ .

When passing from a subspace of  $H_{N_A}$  to another, one finds an identical replica of this spectrum, which amounts to having a degeneracy of the eigenvalues. The degeneracy  $g$  corresponds to the different ways in which one can choose a species  $A$  at a given site provided that  $N$  remains unchanged (i.e., one has the freedom to change singly occupied  $|\uparrow\rangle$  into  $|\downarrow\rangle$  and vice versa); it is therefore easily seen that

$$g(E(\{n_k^A\}; N)) = 2^{2N_A - N} \binom{N_A}{N - N_A}. \quad (8)$$

To conclude this section, we wish to emphasize that the spectrum (7) has been derived by means of the Sutherland species technique under *open* boundary conditions. In fact the same model was also studied under *periodic* boundary conditions,<sup>27</sup> within the algebraic Bethe ansatz approach. However, in the latter case the resulting equations for the quantum numbers do not allow a straightforward evaluation of the eigenvalues; indeed the thermodynamics of Eq. (1) had not been derived yet.

#### IV. THERMODYNAMICS

Thanks to the exact spectrum obtained in the previous section, we can now pass to the study of its thermodynamics, through the exact calculation of the grand partition function. The language of Sutherland's species turns out to be very useful to this aim; indeed, due to the rearrangement of the Fock space described above, one can write

$$\begin{aligned}
\mathcal{Z} &= \text{Tr}(e^{-\beta(\mathcal{H}-\mu\hat{N})}) \\
&= \sum_{\{n_k^A\}} \sum_{N=N_A}^{2N_A} 2^{2N_A-N} \binom{N_A}{N-N_A} \\
&\quad \times \exp\left(-\beta\left[\sum_{k=1}^L (-2t \cos k - U)n_k^A\right] - \beta(U-\mu)N\right) \\
&= \sum_{\{n_k^A\}} (2 + e^{-\beta(U-\mu)})^{N_A} \exp\left(\sum_{k=1}^L [\beta(2t \cos k + \mu)]n_k^A\right) \\
&= \prod_{k=1}^L (1 + \exp\{\beta[2t \cos k + \mu + \nu(U, \beta, \mu)]\}), \quad (9)
\end{aligned}$$

where we have defined  $\nu(U, \beta, \mu) = \ln(2 + e^{-\beta(U-\mu)})/\beta$ ,  $\beta = 1/(k_B T)$  being the inverse temperature and  $\mu$  the chemical potential as usual.

The grand potential is easily obtained as  $\omega = \omega(\beta; U; \mu) = -\lim_{L \rightarrow \infty} \beta^{-1}(\ln \mathcal{Z}/L)$ . After introducing  $\mu_{eff} = \mu + \nu$ ,  $\omega$  reads

$$\begin{aligned}
\omega(\beta; U; \mu) \\
&= -\frac{1}{\pi\beta} \int_0^\pi dk \ln(1 + \exp\{\beta[2t \cos k + \mu_{eff}(U, \beta, \mu)]\}). \quad (10)
\end{aligned}$$

Remarkably, the grand potential is formally similar to that of a tight-binding model with an *effective* chemical potential  $\mu_{eff}$ . We stress that  $\mu_{eff}(U, \beta, \mu)$  depends on the on-site Coulomb repulsion, the temperature, and the chemical potential in a highly nonlinear way. This yields peculiar features of the model, as we shall show in the following.

In deriving the thermodynamics of the system, it is customary to eliminate  $\mu$  in favor of the filling  $\rho$ ; the latter can be computed as  $\rho = -\partial\omega/\partial\mu$ , and the result turns out to be of the following form:

$$\rho(U, \beta, \mu) = [1 + C(U, \beta, \mu)]\rho_A(\beta, \mu_{eff}(U, \beta, \mu)), \quad (11)$$

where

$$C(U, \beta, \mu) = \frac{\exp[-\beta(U-\mu)]}{2 + \exp[-\beta(U-\mu)]} \quad (12)$$

and

$$\rho_A(\beta, \mu_{eff}) = \frac{1}{\pi} \int_0^\pi \frac{dk}{1 + \exp[\beta(-2t \cos k - \mu_{eff})]}. \quad (13)$$

Notice that differentiating  $\omega$  with respect to  $\mu_{eff}$  instead of to  $\mu$  would yield only the right factor  $\rho_A$  of Eq. (11); the

nonlinearity of  $\nu$  as a function of  $\mu$  results in the appearance of  $C$  in the left factor; this causes the relation  $\mu = \mu(\rho; T; U)$  implicitly defined by Eq. (11) to be very different from that of a tight-binding model, as we shall explicitly show in next section.

The two factors in Eq. (11) deserve some comment:  $\rho_A$  is nothing but the density of  $A$  sites along the chain, defined as  $\rho_A = \lim_{L \rightarrow +\infty} \langle \hat{N}_A \rangle / L$ ; the functional dependence of  $\rho_A$  on  $\beta$  and  $\mu_{eff}$  is that of a spinless tight-binding model. The left factor provides information, through the function  $C$ , about the kind of occupancy of the sites of the chain; indeed when  $C \sim 0$  most of the occupied sites are singly (*s*) occupied, whereas if  $C \sim 1$  most of the occupied sites are doubly (*d*) occupied; intermediate values indicate the percentage of *d* with respect to *s* sites.

To conclude this section we wish to comment about the energy (per site) of the system; the latter is obtained by  $\mathcal{E} = -\lim_{L \rightarrow \infty} \partial(\ln \mathcal{Z}/L)/\partial\beta + \mu\rho$  and reads

$$\begin{aligned}
\mathcal{E}(U, \beta, \mu) \\
&= \frac{1}{\pi} \int_0^\pi dk \frac{-2t \cos k - U}{1 + \exp\{\beta[-2t \cos k - \mu_{eff}(U, \beta, \mu)]\}} + U\rho. \quad (14)
\end{aligned}$$

Equation (14) naturally allows one to identify in  $\mathcal{E}$  a kinetic energy  $\mathcal{K}$  and a potential energy  $\mathcal{P}$ . The former is defined as the weighted integral of  $-2t \cos k$  and the latter as the weighted integral of  $-U$ , which actually gives  $-U\rho_A$ , according to Eq. (13). In fact the actual potential energy would also contain the last term  $U\rho$  of Eq. (14); however, since this is merely a constant with respect to temperature, we prefer not to include it in the definition of  $\mathcal{P}$ , so that the latter describes the only temperature-dependent part of the potential term  $U\hat{n}_{i\uparrow}\hat{n}_{i\downarrow}$ . Notice that with this choice the potential energy is attracting for positive  $U$ . Notice also that, although  $\mathcal{K}$  and  $\mathcal{P}$  are clearly related to the hopping terms and to the on-site Coulomb repulsion, respectively, they are not mutually independent: indeed  $\mathcal{K}$  depends not only on  $t$  but also  $U$  and vice versa for  $\mathcal{P}$ . We shall come back to this point in discussing the specific heat in Sec. V.

#### A. Chemical potential

The chemical potential  $\mu(\rho; T; U)$  of our model is shown in Fig. 2 at  $U=t$  (a) and  $U=4t$  (b) for different values of the temperature.

Focusing first on the solid curves, representing the case  $T=0$ , one can realize that even in the ground state the relation between  $\mu$  and  $\rho$  is quite different from that of a spinless tight-binding model, which would read  $\mu(\rho; T=0) = -2t \cos(\pi\rho)$ .

In particular, in Fig. 2(a) we notice that a ‘‘plateau’’ appears, in correspondence with region II of the ground-state phase diagram (see Fig. 1). Interestingly, such a shape reminds us of that of a coexistence region connecting the phase of single carriers (region III-a) to that of pair carriers (region I); this would imply that, as the filling is increased, the 1D lattice starts exhibiting macroscopic regions made of only single carriers separated by other macroscopic regions where only pairs are present. In fact, eigenstates with such features

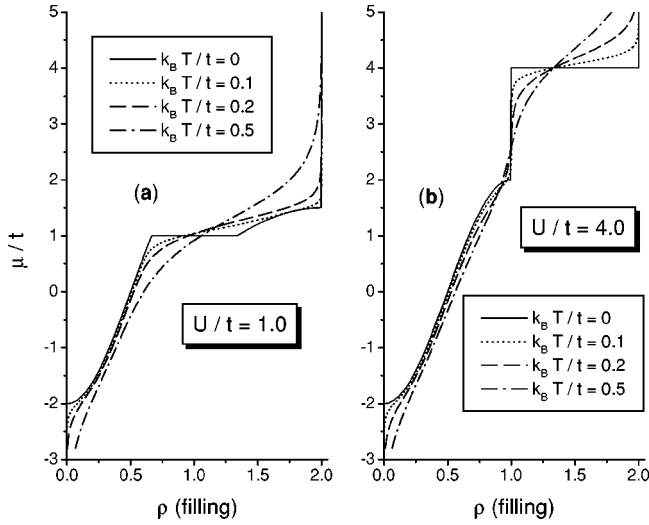


FIG. 2. The relation between  $\rho$  and  $\mu$  for different temperatures at  $U/t=1$  (a) and  $U/t=4$  (b). For  $T=0$ , the curve in (a) shows a plateau, related to “phase coexistence” in mixed region II of Fig. 1, whereas the curve in (b) exhibits a jump in  $\mu$ , due to the opening of charge gap at half-filling.

are certainly present; however, they are degenerate with other eigenstates, in which single and pair carriers alternate with no macroscopic order. This is basically due to the degeneracy of  $A$  sequences in such a region.

In Fig. 2(b) a vertical jump is instead present at half-filling, as a hallmark of the opening of the charge gap. The flat part of the solid curve for  $\rho > 1$  just coincides with the atomic limit behavior (region III-b of Fig. 1).

Considering now the curves at finite temperature of Fig. 2, one can observe how the edges present at  $T=0$  smoothen as soon as  $T > 0$ . A remarkable feature is the presence in Fig. 2(b) of a nearly universal point ( $\rho^* = 4/3$ ,  $\mu^* = U$ ), where all the curves of sufficiently low temperature basically intersect. Such kinds of points are in general determined through the conditions  $\partial\mu/\partial T = 0$  and  $\partial^2\mu/\partial T^2 = 0$ . It is in fact possible to calculate that for any  $U > 2t$  and  $\rho > 1$  (region III-b of Fig. 1) the low-temperature behavior of  $\mu$  is given by

$$\mu \simeq U + k_B T \ln\left(\frac{2(\rho-1)}{2-\rho}\right) + \mathcal{O}(e^{-(U-2t)/k_B T}), \quad (15)$$

whence the above conditions are both fulfilled up to exponentially small terms in  $k_B T/t$ .

We shall also see in Sec. IV D that nearly universal crossing points are exhibited by other observables of the model, such as the specific heat.

Equation (15) also points out that in our model a *linear* low-temperature behavior is possible, differently from the tight-binding model, where only even powers in  $T$  are allowed in the Sommerfeld expansion. In general, in our model, different behaviors of  $\mu$  arise according to the values of  $U$  and  $\rho$ . For instance, for  $U$  and  $\rho$  belonging to the mixed region II of Fig. 1, the chemical potential at low temperature has again a linear term,

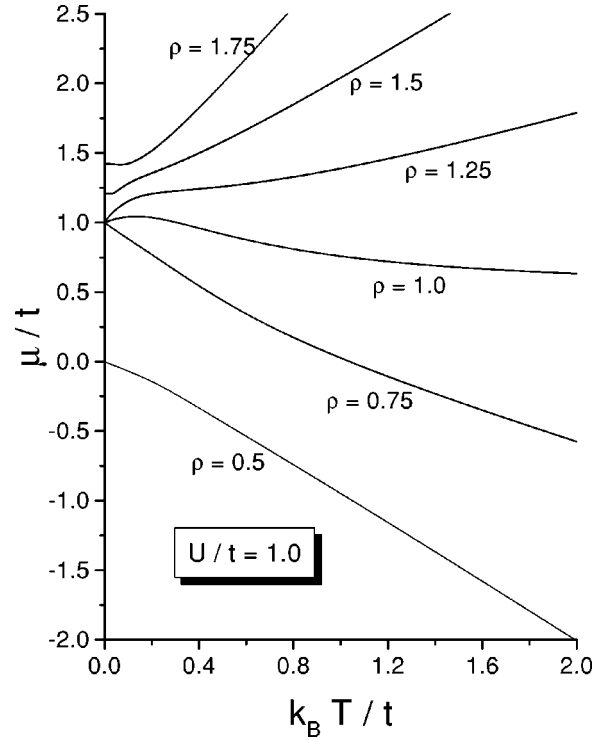


FIG. 3. The behavior of  $\mu$  as a function of temperature for fixed  $U/t=1$  and different values of filling. The asymmetry with respect to the half-filled case  $\rho=1$  is ascribed to the lack of particle-hole invariance of the model.

$$\mu \simeq U + k_B T \ln\left(\frac{2(\rho - \bar{\rho})}{2\bar{\rho} - \rho}\right) + \mathcal{O}((k_B T/t)^2), \quad (16)$$

but with a coefficient which depends on  $U$ , since  $\bar{\rho} = \bar{\rho}(U) = \pi^{-1} \cos^{-1}(-U/2t)$ .

In contrast, when the charge gap  $\Delta_c = U - 2t$  opens (i.e., at  $\rho=1$  and  $U > 2t$ ),  $\mu$  acquires a highly nonlinear form

$$\mu \simeq 2t + \frac{\Delta_c}{2} + \frac{k_B T}{4t} \ln\left(\frac{k_B T}{4\pi t}\right), \quad (17)$$

indicating that the behavior is definitely different to that of an intrinsic semiconductor.

In Fig. 3 we explicitly examine the behavior of  $\mu$  as a function of temperature for a fixed value of on-site Coulomb repulsion ( $U/t=1$ ) and for different fillings. A main difference has to be emphasized with respect to the case of a tight-binding model: in the latter the curves of  $\mu$  are specular for filling values that are symmetric with respect to half filling (i.e.,  $\mu \rightarrow -\mu$  for  $\rho \rightarrow 2-\rho$ ), whereas this is not the case in our model, due to the fact that it is not particle-hole invariant.

## B. Compressibility

The compressibility  $\kappa = \partial\rho/\partial\mu$  can be easily evaluated through Eq. (11). In Fig. 4 we have plotted  $\kappa$  as a function of the temperature for a fixed value of  $U$  (namely,  $U/t=1.0$ ) and for different fillings. One can observe the change in the

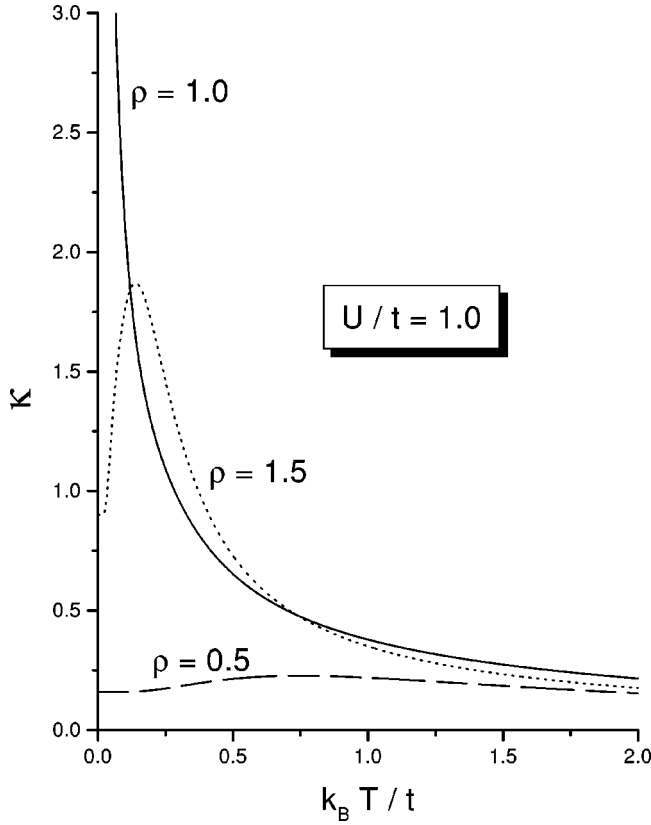


FIG. 4. The compressibility as a function of temperature at fixed on-site Coulomb repulsion  $U/t=1.0$  and for different filling values.  $\kappa$  diverges as  $T \rightarrow 0$  for values of  $U/t$  and  $\rho$  belonging to mixed region II of Fig. 1.

low-temperature behavior when tuning the filling: at  $\rho=0.5$  the behavior is regular, while at half-filling  $\kappa$  undergoes a singularity for  $T \rightarrow 0$ ; eventually ( $\rho=1.5$ ) its behavior is again regular. The reason for the low-temperature singularity at  $\rho=1$  is that in the ground state the point ( $U/t=1; \rho=1$ ) is situated in region II (see Fig. 1), i.e., in the region where the chemical potential exhibits the plateau, as shown in Fig. 2; such a singularity is indeed present for all values of  $U$  and  $\rho$  that belong to that region of the ground state. The divergence of  $\kappa$  can be proved to be of the type  $\propto T^{-1}$ .

In contrast the behavior for  $T \rightarrow 0$  at  $\rho=0.5$  and  $\rho=1.5$  is regular since such filling values belong to regions III-a and I, respectively.

In Fig. 5 we have examined in detail the case of half-filling, plotting  $\kappa$  as a function of  $T$  for different values of  $U$ ; one can explicitly observe how  $U=2t$  is the critical value separating the divergent behavior for  $U < 2t$  from the regular one for  $U > 2t$ . Indeed, as soon as  $U > 2t$ , the divergence becomes a pronounced peak in  $\kappa$ ; the temperature  $T^*$  at which the peak occurs increases with increasing  $U$ , similarly to what happens in the ordinary Hubbard model, according to the results of Ref. 12. Notice that in contrast no singular behavior is expected at moderate  $U$ 's in the ordinary Hubbard model at half-filling, since in that case the system is insulating for any positive  $U$ .

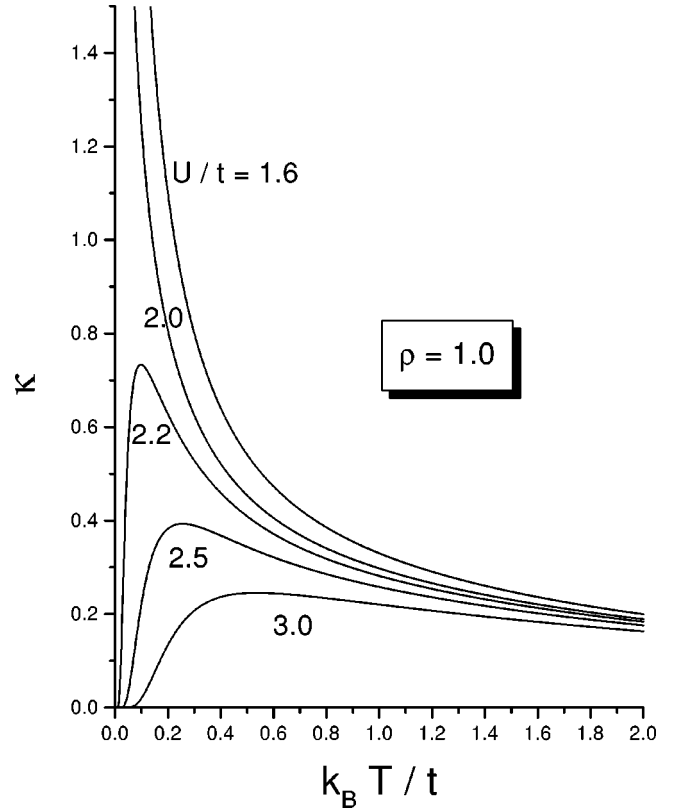


FIG. 5. The compressibility as a function of temperature at fixed filling  $\rho=1$  and for several values of on-site Coulomb repulsion. As the charge gap opens ( $U > 2t$ ),  $\kappa$  acquires an exponential low-temperature behavior.

### C. Local magnetic moment

The local magnetic moment was first introduced in Ref. 14 and is defined as

$$\lambda_0 = \lim_{L \rightarrow \infty} \left\langle \frac{1}{L} \sum_j (\hat{n}_{j\uparrow} - \hat{n}_{j\downarrow})^2 \right\rangle. \quad (18)$$

It characterizes the magnitude of spin at each site, i.e., the degree of localization of electrons. In terms of the density of  $A$  sites,  $\lambda_0$  can be easily rewritten as  $\lambda_0 = \rho - 2\rho_{\uparrow\downarrow} = 2\rho_A - \rho$ , where  $\rho_A$  can be computed from Eq. (13). In Fig. 6 we have reported the local magnetic moment at half-filling for different values of the on-site Coulomb repulsion. One can observe that the behavior of  $\lambda_0$ , even within a relatively small range of values of  $U$ , is quite rich. In order to describe it, we first consider the case of small values of  $U$  (namely,  $U = 1.4t$  in the figure); we recall that in the ground state such a value corresponds to the mixed region II (see Fig. 1 at  $\rho = 1$ ), meaning that hopping paired electrons are present at  $T=0$ ; as the temperature is turned on,  $\lambda_0$  first increases with  $T$  (indicating that the pairs are broken in favor of single carriers); however, after reaching a maximum at a temperature  $T^*$ ,  $\lambda_0$  starts decreasing for higher  $T$ 's, denoting that pairs are now reformed by higher thermal excitations. According to the above observations, it is easy to realize that the temperature  $T^*$  decreases with increasing  $U$ ; in fact the

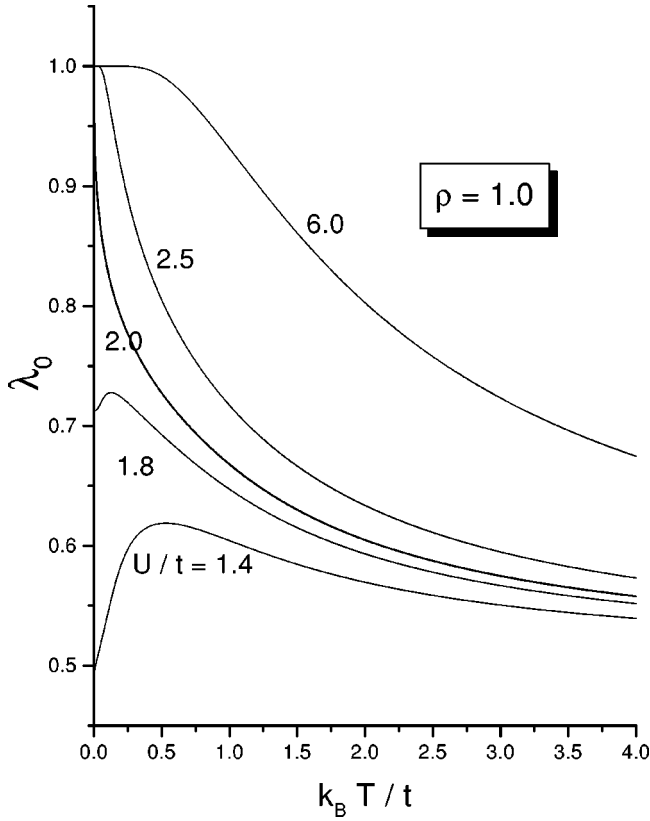


FIG. 6. Local magnetic moment as a function of the temperature at half-filling for several values of  $U/t$ . Notice how the low-temperature behavior abruptly changes across the metal-insulator transition point. The figure indirectly provides also the behavior of  $\rho_A$ , since  $\lambda_0 = 2\rho_A - \rho$ .

maximum disappears for  $U \approx 1.85$ , so that  $\lambda_0$  becomes a definitely decreasing function of the temperature. At  $U = 2t$ ,  $\lambda_0$  reaches at  $T=0$  the saturation value 1 (all singly occupied sites), with an infinite derivative with respect to the temperature. Passing through  $U = 2t$ , an abrupt change in the low-temperature slope occurs: the curve of  $\lambda_0$  suddenly flattens as soon as  $U > 2t$ . This reflects the metal-insulator transition occurring in the ground state; indeed the opening of the charge gap causes the formation of pairs to be highly unfavored at low  $T$ 's.

#### D. Specific heat

In this subsection we present our results on the specific heat of model (1) which can be computed through

$$C_V = \frac{d\mathcal{E}}{dT} = -k_B \beta^2 \left( \frac{\partial \mathcal{E}}{\partial \beta} - \frac{\partial \mathcal{E}}{\partial \mu} \frac{\partial \rho}{\partial \beta} \right) / \frac{\partial \rho}{\partial \mu}, \quad (19)$$

where the energy  $\mathcal{E}$  is given by Eq. (14). Below we study the temperature dependence of  $C_V$  when varying the physical parameters  $U$  and  $\rho$ . The exact calculation shows that in our model a two-peak structure is definitely present not only in the strong-coupling regime, but also at moderate  $U$ 's.

We start by considering the case of half-filling ( $\rho = 1$ ). The two peaks appear first for  $1.3 \lesssim U/t \lesssim 1.8$  (see Fig. 7); in

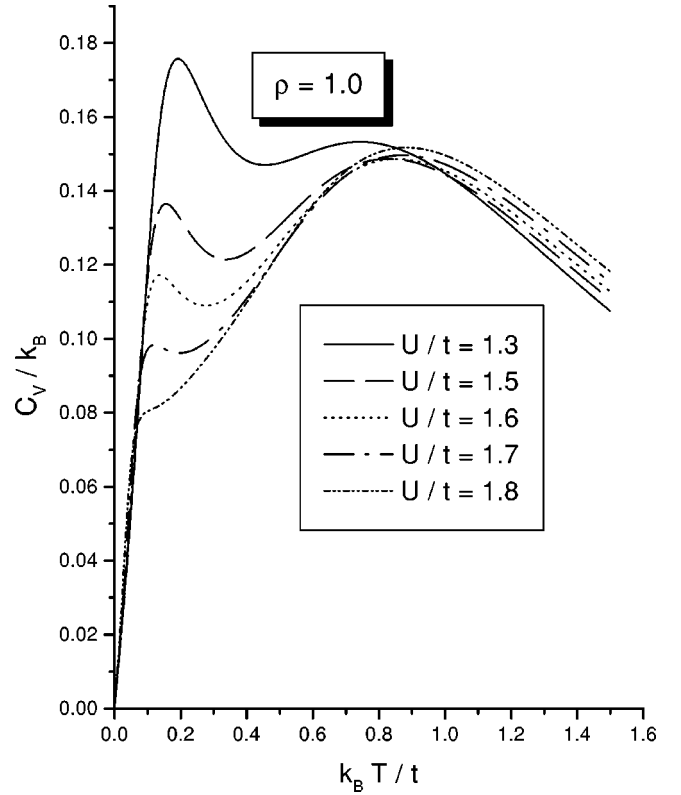


FIG. 7. Specific heat as a function of  $T$  at half filling for different values of  $U/t$  below the metal-insulator transition value: a two-peak structure is present, as well as a nearly universal crossing point. The low-temperature behavior is linear.

this range of  $U$ 's,  $C_V$  also exhibits a nearly universal crossing point at  $k_B T \sim 0.85t$ ; we shall comment on such feature at the end of this subsection. The peaks eventually merge into one for  $U/t \sim 1.85$ . However, as soon as  $U > 2t$  (see Fig. 8), a new well-pronounced low-temperature peak appears. The recovered double-peak structure is present up to  $U \sim 3t$ , where finally only one peak survives.

By comparing Figs. 7 and 8, one can notice that the metal-insulator transition point  $U = 2t$  is also the hallmark of a crossover in the low-temperature behavior of  $C_V$ . In particular, the calculation shows that for  $U < 2t$  the latter is linear,

$$C_V \approx \frac{k_B}{2\pi\sqrt{1-(U/2t)^2}} \left( \frac{\pi^2}{3} + \ln^2 \frac{4(1-\bar{\rho})\bar{\rho}}{(2\bar{\rho}-1)^2} \right) \frac{k_B T}{t}, \quad (20)$$

where  $\bar{\rho}$  is defined as in Eq. (16). In contrast, for  $U > 2t$ ,  $C_V$  exhibits an exponential-like behavior given by

$$C_V \approx \frac{k_B}{(4\pi)^{1/4}} \left( \frac{\Delta_c}{2t} \right)^2 \left( \frac{k_B T}{t} \right)^{7/4} \exp\left( -\frac{\Delta_c}{2k_B T} \right), \quad (21)$$

where  $\Delta_c = U - 2t$  is the charge gap.

To conclude the study at half-filling we have examined the case of large  $U/t$  (see Fig. 9). The result shows that only one peak is present, at a temperature which increases almost



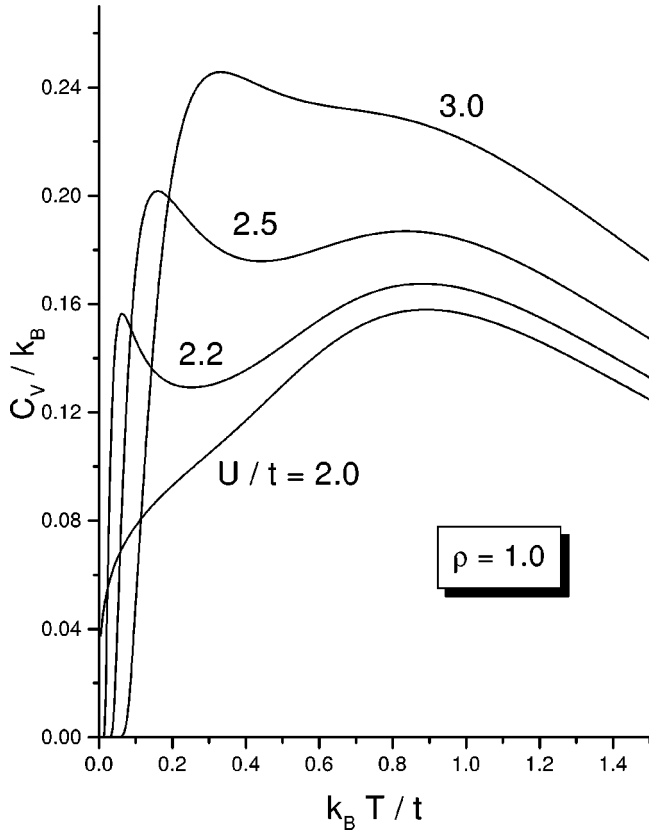


FIG. 8. Specific heat as a function of  $T$  at half filling and different values of  $U/t$  just above the metal-insulator transition point: the two-peaks structure definitely disappears for  $U \geq 3t$ . The low-temperature behavior is exponential for  $U > 2t$ .

linearly with  $U$  ( $k_B T \sim 0.21U$ ). This result can be understood considering that at large  $U/t$  the spectrum (7) exhibits two different energy scales: (i) a low-energy scale ( $\sim t$ ), which describes fluctuations in the  $A$  band, whose effective filling is given by the value of  $\rho_A$ , and (ii) a high-energy scale (of the order of  $U$ ) involving the formation of on-site pairs, favoring the decrease of the number of  $A$  sites. The former channel is actually active only for  $\rho < 1$ , since at half-filling the  $A$  band becomes completely filled: indeed in this case we have  $\rho_A \approx 1$  for  $k_B T \sim t$ , as can be deduced from Fig. 6 of the local magnetic moment at large  $U/t$ .

Only the high-energy channel is thus active, and its contribution is well described by the atomic-limit model (i.e.,  $t = Y = 0$ ), shown by the dotted curve in Fig. 9. The slight deviations are due to the fact that, as pairs are formed from singly occupied sites via thermal fluctuations, the number of effective species  $A$  decreases, and the formed  $A$  holes can produce (relatively small) fluctuations with  $T$ . However, the larger is  $U/t$ , the better is the agreement with the specific heat of the atomic limit.

We also wish to emphasize that the behavior is different from that of the ordinary Hubbard model, where two peaks appears at low temperatures in the strong-coupling limit at half-filling. In fact, although in the Hubbard model the lower Hubbard band is filled, spin excitations of low energy ( $\sim J$

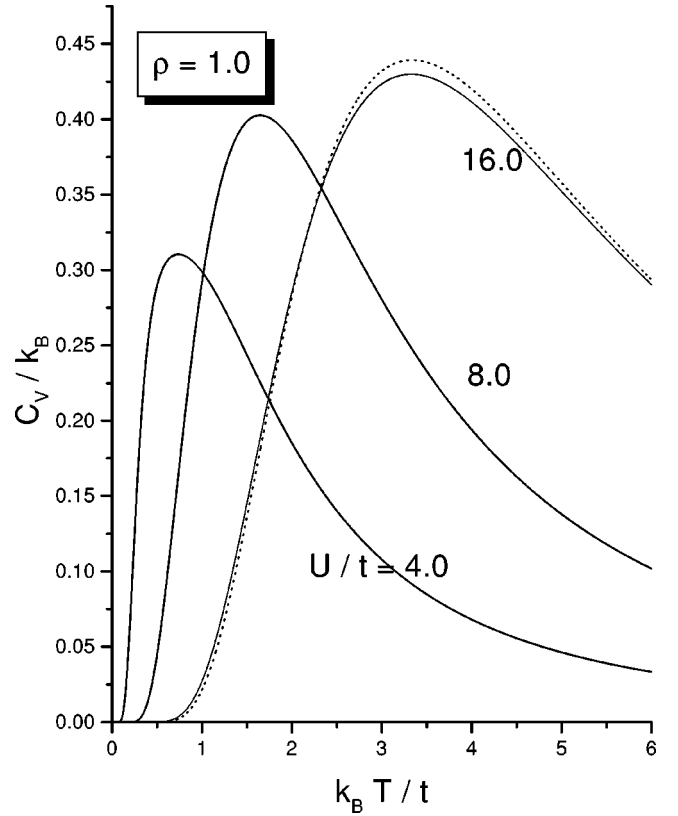


FIG. 9. Specific heat as a function of  $T$  for half-filling and  $4t \leq U \leq 16t$ . In the strong-coupling regime, the two-peak structure disappears: the remaining peak is well described from the atomic-limit model (dotted curve). A similar behavior is obtained also at any  $\rho > 1$ .

$= 4t^2/U$ ) are active. These kind of excitations are instead absent in our model; we shall comment in more detail in Sec. V about this point.

In Fig. 10 we investigate the specific heat for filling values below half-filling: namely,  $\rho = 0.75$ .

As Fig. 10(a) shows, a double-peak structure of  $C_V$  appears; however, two important differences have to be emphasized with respect to the case of half-filling: in the first instance, here the double-peak structure arises and becomes more evident for *large* values of  $U$ 's, whereas at half-filling it is present at *moderate*  $U$ 's; second, the temperatures of the two peaks are quite higher than the corresponding ones of the half-filled case. In particular the position of the low-temperature peak is practically independent of  $U$ , whereas the high-temperature one strongly depends on it, similarly to what happens for the only peak present at half-filling in the strong-coupling regime (Fig. 9).

The two peaks of Fig. 10(a) have to be related to the two energy scales emerging in the spectrum when  $U \gg t$ , as discussed above; in particular, the low-temperature one is attributed to the fluctuations of the  $A$  band, which is now partially filled, unlike for half-filling. We recall that in this range of the parameters  $U$  and  $\rho$ , the ground state of the model is that of the  $U = \infty$  model (region III-a of Fig. 1); since the formation of pairs is strongly inhibited for high  $U$ 's, the physics of low-energy excitations is fairly captured by that of the  $U$

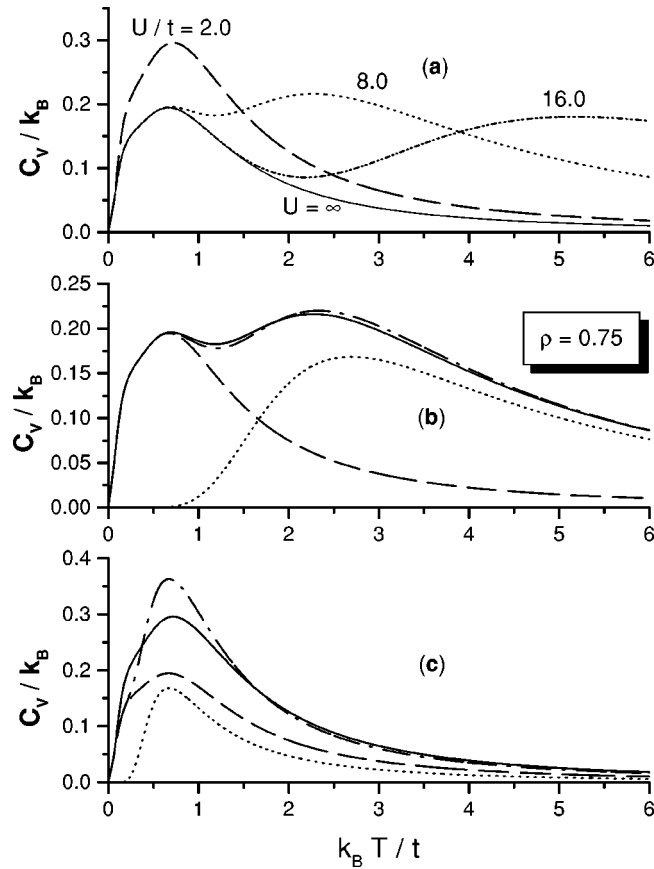


FIG. 10. The specific heat as a function of temperature for  $\rho = 0.75$ . In (a),  $C_V$  is plotted for different values of  $U/t$ ; (b) at strong coupling ( $U/t=8$ ) the specific heat of the model (solid line) is well reproduced by the sum (dot-dashed line) of the specific heat of the  $U=\infty$  model (dashed line) and of the atomic limit (dotted line); (c) this is not the case at moderate coupling, where the energy scales of the two models become comparable ( $U/t=2$ ).

$=\infty$  model at finite temperature, as shown by the solid curve in Fig. 10(a). In Fig. 10(b) the case  $U/t=8$  is examined in detail; in this case the sum of the specific heats of  $U=\infty$  model and atomic model practically recovers the actual  $C_V$  of our model. Such agreement improves with increasing  $U$ , whereas at moderate values of  $U$  the argument of energy scale separation does not hold: indeed the high-temperature peak merges into the low-temperature one for  $U\sim 2t$ , and  $C_V$  is no longer given as the sum of  $U=\infty$  and atomic limits [see Fig. 10(c)].

We have also considered the case of filling values greater than 1. In the strong-coupling regime the ground state has the  $A$  band completely filled, the sites of the chain being all occupied (either singly or doubly, as shown in region III-b of Fig. 1); the low-energy scale is thus frozen, just like in the case of half-filling. This yields the specific heat behavior to be actually described by that of the atomic limit, similarly to Fig. 9. The temperature of the peak grows linearly with  $U$  [ $k_B T \approx c(\rho)U$ ], the coefficient  $c$  being an increasing function of the filling  $\rho$ .

Figures 11 and 12 examine the filling dependence of the specific heat at fixed coupling values. More precisely, Fig. 11

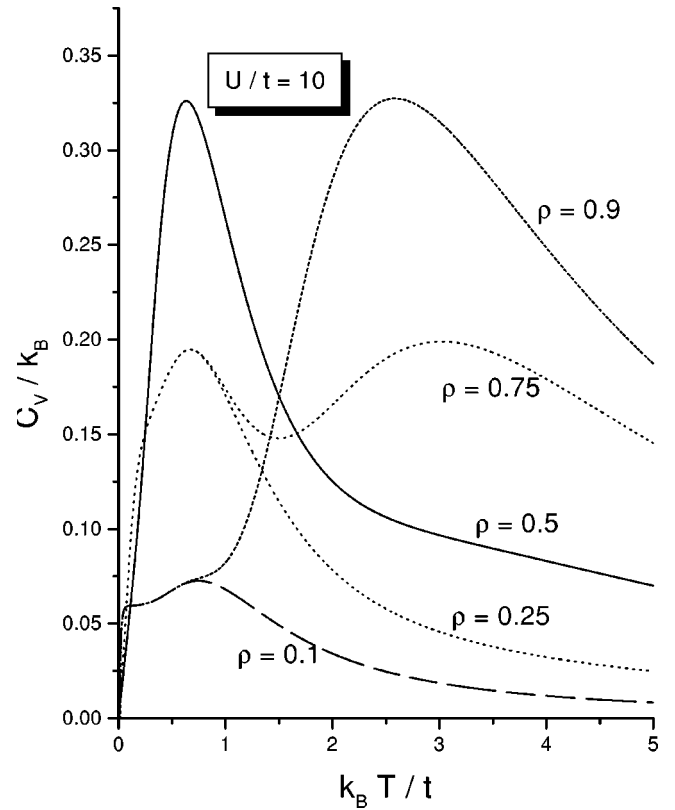


FIG. 11. The specific heat as a function of temperature at strong coupling and  $\rho < 1$ . The low-temperature behavior is the same for values of  $\rho$  symmetric with respect to  $\rho=0.5$ : indeed in this case low-energy excitations are well described by the  $U=\infty$  Hubbard model, which is particle-hole invariant around quarter-filling. Differences instead emerge at high temperatures.

reports the results obtained in the strong-coupling case. As anticipated above, in this case the low-temperature peak is perfectly recovered from the  $U=\infty$  model; notice that, since the latter is particle-hole symmetric around quarter-filling ( $\rho=0.5$ ), the low-temperature behavior of curves related to filling values that are symmetric with respect to  $\rho=0.5$  is basically identical. In contrast, the higher-temperature peak does not exhibit such symmetry, being related to the atomic limit of the Hubbard model, which is no more particle-hole symmetric around quarter-filling.

Figure 12 is concerned with the behavior at moderate  $U$ 's (namely,  $U/t=1.5$ ) as a function of  $\rho$ ; the remarkable feature is the appearance of a nearly universal crossing point at low temperature ( $k_B T \sim 0.2t$ ) for a finite range of filling values ( $1.0 \leq \rho \leq 1.3$ ). Similarly, a nearly universal crossing point also occurs at fixed filling for varying  $U$ , as Fig. 7 shows. The latter type of behavior is also exhibited by the ordinary half-filled Hubbard model;<sup>12,13,17,18</sup> however, to the authors' knowledge, theoretical investigations were mostly limited to the case of fixed filling and varying  $U/t$ . In contrast, here we have explored the case of varying  $\rho$  as well; this is interesting in view of a comparison with experimental results, where  $U/t$  can be roughly interpreted as the inverse pressure and  $\delta = |1 - \rho|$  as the doping. In fact, this type of universal behavior has been observed in many heavy-fermion com-

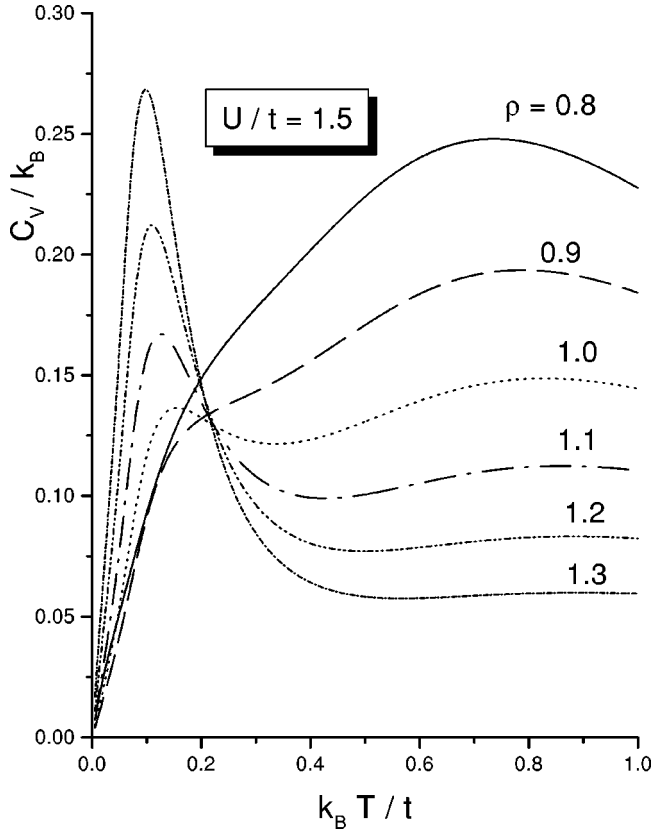


FIG. 12. The specific heat as a function of temperature in the moderate- $U$  regime. A nearly universal crossing point with varying  $\rho$  at fixed  $U$  is observed for values of  $\rho$  in the range  $0.9 \leq \rho \leq 1.3$ .

pounds, such as the cerium ones, both at fixed doping with varying pressure,<sup>19</sup> and at fixed pressure with varying doping.<sup>20</sup> Let us notice that, for the ordinary Hubbard model, the presence of the nearly universal point in  $U$  has been explained in Ref. 35, as a consequence of the fact that the entropy  $S$  at high temperatures does not depend on  $U$ , in that case. For our model,  $S$  at high temperatures is also independent of  $U$ ; however, it turns out that it *does* depend on  $\rho$ . Hence we expect that the argument in Ref. 35 cannot be applied to explain the nearly universal crossing point in  $\rho$  shown in Fig. 12.

Finally, the specific heat  $C_V$  is investigated in Fig. 13 also for negative values of the Coulomb interaction, at half-filling. The behavior is quite different with respect to the positive- $U$  case for moderate and intermediate  $U$  values, since no double peak is present.

In contrast, such structure emerges at higher coupling values; also in this case two separate energy scales emerge. However, the low-temperature peak is now reproduced by that of the  $XX0$  model ( $t=0$ ), whose ground state actually coincides with that of our model, for these values of  $U$  and  $\rho$  (see region I in Fig. 1). The high-temperature peak is still due to the negative- $U$  atomic limit ( $t=Y=0$ ). In Fig. 13(b) it is clearly shown how, in the strong-coupling case, the simple sum of the specific heats of  $XX0$  and atomic limit perfectly reproduces the result for our model; this is not the case by at lower  $U$  values.

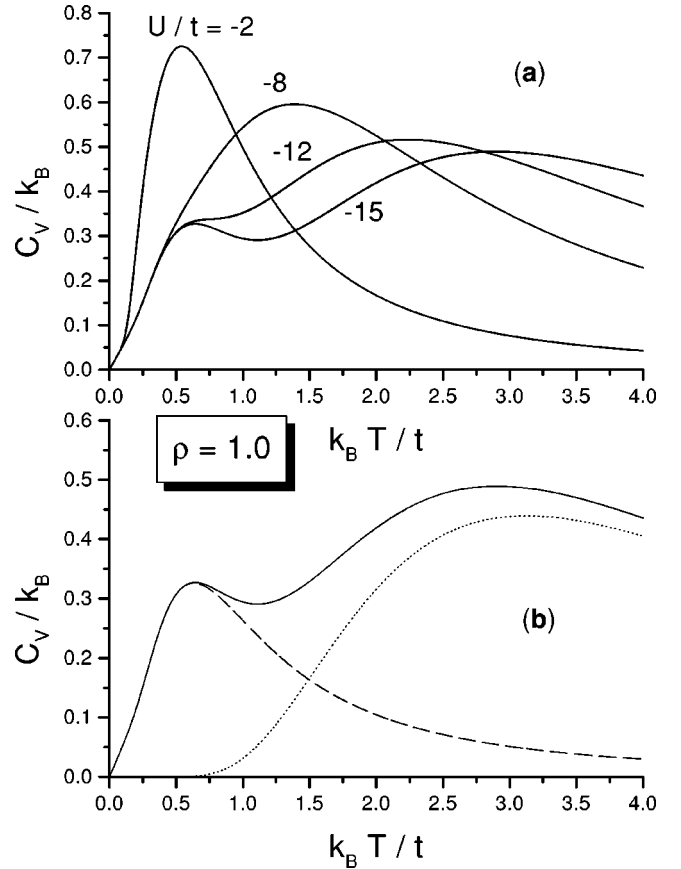


FIG. 13. The specific heat as a function of temperature at half-filling for negative values of  $U$ . (a) The double peak emerges as  $|U|$  is increased. (b) In the strong-coupling regime ( $U/t = -15.0$ ),  $C_V$  is fairly reproduced by the sum of the  $XX0$  contribution (dashed line) and the atomic limit contribution (dotted line).

## V. DISCUSSION

As outlined in the previous section, our results show that the specific heat exhibits a two-peak structure for different values of on-site Coulomb repulsion  $U$  and filling  $\rho$ . In the present section we wish to discuss the origin of the two peaks, since in the last few years much effort has been made to clarify a similar behavior occurring in the ordinary Hubbard model. As mentioned in the Introduction, in the latter model the two peaks are usually explained in terms of “spin” and “charge” excitations.

The above argument cannot be applied here, since our model involves only charge degrees of freedom: in fact, from the *formal* point of view of quantum numbers  $n_k^A$ , the excitation processes in the spectrum (7) have the typical feature of charge excitations (in the sense of  $A$  species). It is, however, worth emphasizing that, just like for the ordinary Hubbard model, the nomenclature based on quantum numbers does not strictly correspond to its *physical* meaning. In our case, the charge degrees of freedom of  $A$  species actually carry both *charge* and *spin* density fluctuations: the breakup of a localized pair into two single carriers indeed leads to a redistribution of the charge density as well as to the formation of a triplet replacing a singlet state.

In our model any peak of the specific heat has thus to be

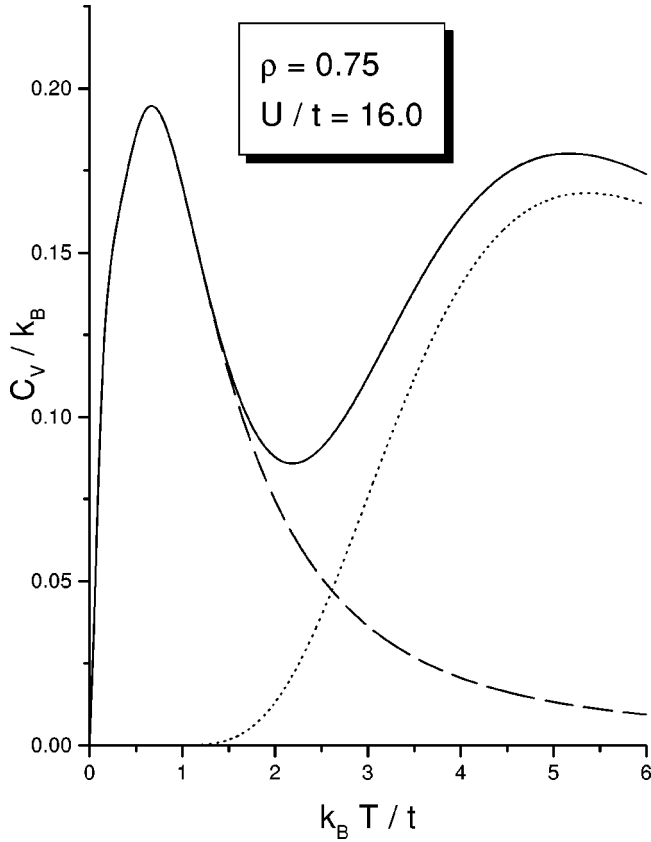


FIG. 14. The kinetic (dashed line) and potential (dotted line) contributions to the specific heat (solid line) at strong coupling ( $U/t=16$ ) for  $\rho=0.75$ . The low-temperature peak is basically due to  $\mathcal{K}'$ , while the high-temperature peak stems from  $\mathcal{P}'$ . In this regime ( $U \gg t$ ),  $\mathcal{K}'$  is also well described by the specific heat of  $U = \infty$  Hubbard model and  $\mathcal{P}'$  by that of the atomic limit (dashed and dotted curves of Fig. 10).

ascribed just to charge excitations. We have seen in Sec. IV D that, when varying the parameters  $U$  and  $\rho$ , the peaks can merge into one and possibly reappear. In the following we shall discuss such a structured behavior through the kinetic and potential contributions to  $C_V$ : namely, the derivatives  $\mathcal{K}'$  and  $\mathcal{P}'$  with respect to the temperature of  $\mathcal{K}$  and  $\mathcal{P}$ , defined when giving the internal energy (14).

We start by the case of the strong coupling ( $U \gg t$ ), where our results show a two-peak structure for positive  $U$  and  $\rho < 1$  [see Fig. 10(b)], as well as for negative  $U$  at any filling [see Fig. 13(b)]. Since in these regimes the characteristic energy scales of the kinetic term ( $t$ ) and the potential term ( $U$ ) of the Hamiltonian are well separated, it is expected that each of the two peaks is related to one of these terms. In Fig. 14 we have thus plotted  $\mathcal{K}'$  and  $\mathcal{P}'$  for  $U/t=16$  and  $\rho = 0.75$ : the two peaks are indeed in perfect correspondence with the contributions of  $\mathcal{K}$  and  $\mathcal{P}$ . It is also worth stressing that these two contributions can be quite well described at strong coupling in terms of two different models: explicitly, the low-temperature kinetic behavior is captured by the  $U = \infty$  model for positive  $U$ 's [Fig. 10(b)] and by the  $XX0$  model for negative  $U$ 's [Fig. 13(b)]; the high-temperature potential behavior is instead described by the atomic limit.

In contrast, in the regime of moderate  $U$ 's the two energy scales become comparable, and the above argument is not applicable. This gives rise to a completely different scenario; for instance, at half-filling we observe that by lowering  $U$  the single strong-coupling peak splits into two, whereas for  $\rho < 1$  the two strong-coupling peaks merge into a single one. In practice, while for  $|U| \gg t$  the kinetic and potential terms decouple, at moderate  $U$ 's it is the *competition* between the two kinds of energy that determines the actual shape of the specific heat.

This can be understood by recalling the structure of the energy spectrum [see Eq. (7)]; both terms can be expressed in terms of the quantum numbers  $n_k^A$ , where the total number of  $A$  sites is not a fixed quantity, but can vary in the range  $N_A \in [N/2; N]$  (the electron number  $N$  being obviously fixed). This property actually yields the competition between  $\mathcal{P}$  and  $\mathcal{K}$ : indeed the kinetic term may favor the decrease of  $N_A$ , in order to eliminate possible positive contributions of  $-2t \cos k$ , whereas the potential term favors the increase of  $N_A$  (i.e., the breaking of on-site pairs). This competition is already active at  $T=0$ , causing the appearance of the different regions in the ground-state phase diagram.

At finite temperature two more mechanisms enter driving such competition: (i) the density  $\rho_A$  of  $A$  carriers varies with  $T$ , according also to the values of  $U$  and  $\rho$ , and (ii) the kinetic term exhibits the usual thermal fluctuations. The former represent the crucial difference with respect to an ordinary free spinless fermion model, where only thermal excitations are present, at *fixed* number of carriers. Notice also that the variability of  $\rho_A$  can happen to contrast the effect of thermal fluctuations: this is the case when  $\rho_A$  decreases with  $T$ , since this would yield a reduction of  $\mathcal{K}$ , while thermal fluctuations would lead to an increase of it. As a consequence, a further competition, concerned with the purely kinetic contribution, may occur.

In Fig. 15 we plot the derivatives  $\mathcal{K}'$  and  $\mathcal{P}'$  of the kinetic and potential parts for various moderate  $U$ 's at half-filling. Starting from  $U/t=1.6$  we observe that at low temperatures both  $\mathcal{K}'$  and  $\mathcal{P}'$  exhibit a peak at nearly the same temperature  $T_1$ ; this is due to the fact that in this regime they are driven by the same mechanism (formation of pairs from singly occupied sites). The two contributions of opposite signs do not completely cancel each other; the kinetic one prevailing, a kinetic low-temperature peak appears in  $C_V$ . Notice that the value of  $C_V$  at the peak is relatively small with respect to that of  $\mathcal{K}'$  and  $\mathcal{P}'$ ; this is just the hallmark of a competition between the two contributions.

At a higher temperature  $T \approx T_2$ , located in between the two peaks of  $C_V$ ,  $\mathcal{K}'$  has a flat minimum and  $\mathcal{P}'$  a flat maximum. Finally, at still higher values of temperature,  $\mathcal{K}'$  exhibits a second maximum at  $T_3$ , and  $\mathcal{P}'$  is smoothly decreasing; in correspondence,  $C_V$  exhibits the second peak, of kinetic origin.

As  $U$  is increased [Fig. 15(b)], the value of  $T_1$  decreases and the absolute height of both the above contributions drastically vanishes, so that the low-temperature peak becomes a sort of “shoulder.” At the same time, the minimum of the kinetic contribution and the maximum of the potential con-

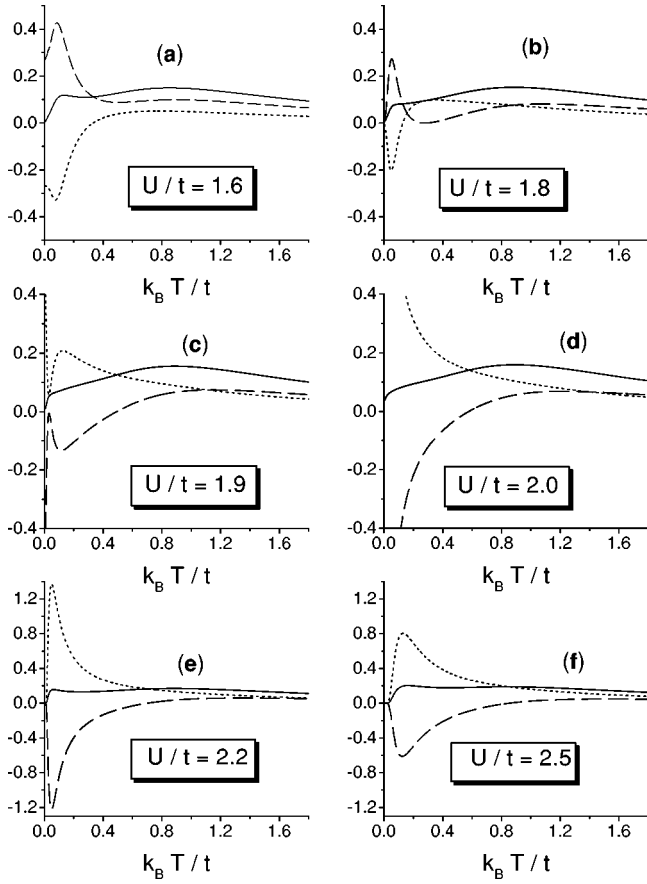


FIG. 15. The temperature dependence of the kinetic (dashed line) and potential (dotted line) contributions to the specific heat (solid line), in units of  $k_B$ , at half-filling and different moderate values of  $U$ . Contrary to the case  $U \gg t$  of Fig. 14, at moderate coupling  $\mathcal{K}'$  and  $\mathcal{P}'$  are competing, since they have relatively large contributions of opposite signs at roughly the same temperature. The peaks of  $C_V$  are thus “kinetic” (“potential”) when  $\mathcal{K}'$  ( $\mathcal{P}'$ ) prevails on the other. Notice that the low-temperature peak changes its origin from kinetic to potential across the metal insulator transition point; the high-temperature one, present up to  $U/t \approx 2.5$ , is instead always of kinetic origin. (For editing reasons the two bottom figures have a different y-axis scale.)

tribution located around  $T_2$  have become more pronounced, and  $T_2$  itself has decreased [see Fig. 15(c)]. As  $U$  reaches the value  $2t$  of the metal-insulator transition, both  $T_1$  and  $T_2$  vanish and the magnitude of the corresponding extrema becomes infinite [Fig. 15(d)]. For  $U > 2t$  [Figs. 15(d) and 15(e)], the  $T_2$  extrema are regularly restored and, since the  $T_1$  extrema have disappeared, they become the new low-temperature extrema. At this temperature  $C_V$  exhibits now a new peak. Thus, for  $U > 2t$ , the potential contribution prevails on the kinetic one, and the nature of the low-temperature peak changes with respect to the case  $U < 2t$ . Notice that  $T_2$  now increases with  $U$  [Figs. 15(e) and 15(f)]. Finally, at higher temperatures another broad peak originates from the (old) second maximum of the kinetic part. Such a high-temperature ( $T_3$ ) peak is very broad, and it definitely disappears when  $U$  is further increased above  $3t$ .

The above observations show that at half-filling, passing

through the point  $U = 2t$  of the metal-insulator transition, the nature of the low-temperature peak changes its origin from a kinetic to a potential one, whereas at moderate  $U$ 's a further peak of kinetic origin appears at higher temperatures. In passing let us also notice that at strong coupling a kinetic (potential) peak is a peak to which only  $\mathcal{K}'$  ( $\mathcal{P}'$ ) basically contributes,  $\mathcal{P}'$  ( $\mathcal{K}'$ ) being almost vanishing (see Fig. 14); in contrast, at moderate  $U$ 's a kinetic (potential) peak is a peak for which the kinetic contribution slightly prevailing on the potential (kinetic) one.

The results obtained for our model can be compared with those concerning the ordinary Hubbard model. In the strong-coupling regime of this model the low-temperature peak is attributed to spin excitations (the corresponding temperature being of the order of  $J = 4t^2/U$ ), whereas the high-temperature peak is related to the charge excitations (since it is located at  $k_B T \sim U$ ). With lowering  $U$ , it is widely accepted that the two peaks merge at  $U \approx 4t$ ; however, some investigations have been carried out at still lower  $U$ 's, showing that a double-peak structure reappears for  $D = 1$  (Ref. 11) and  $D = 2$  (Refs. 16 and 17). It is customary to relate the origin of these new peaks again to spin and charge degrees of freedom, respectively.

The Hubbard model is considered the paradigm within strongly correlated systems, so that the presence of a two-peak structure in the specific heat of such systems tends naturally to be interpreted as the signature of spin and charge excitations.

However, in the authors' opinion, not enough attention has been devoted to the effect that further interaction terms in the Hamiltonian have on the specific heat. To this purpose, the exact results obtained for our model show that, when a possible competition between single and paired carriers is taken into account, the specific heat turns out to exhibit a structured two-peak behavior, in spite of the fact that only charge degrees of freedom are involved. Although our model neglects some terms such as the nearest-neighbor charge interaction ( $\sim V \hat{n}_{i\sigma} \hat{n}_{j\sigma'}$ ), we believe that it can reproduce some features of realistic materials which are not explicitly taken into account in the ordinary Hubbard model: namely, (a) the opening of the gap at a *finite* value of  $U/t$ , i.e., at a finite value of pressure on the sample; (b) the lack of particle-hole symmetry, observed in heavy-fermion compounds; and (c) the presence of a mechanism favoring the kinetic of paired carriers, as is the case in cuprate superconductors. In view of these observations, we suggest that the interpretation of a two-peak structure in  $C_V$  may not necessarily be related to spin and charge excitations; a comparison with the behavior of pure spin quantities, such as magnetic susceptibility, in correspondence of the peaks temperature would be more probative.

## VI. CONCLUSIONS

In this paper we have calculated the exact thermodynamics of an extended Hubbard model by means of the Sutherland species technique, which we had previously introduced to determine the ground-state properties of the same model.<sup>1</sup> The model describes a competition between the dynamics of

single carriers and that of short-radius paired carriers; such competition is modulated by the values of the electron filling  $\rho$  and on-site Coulomb repulsion  $U$ . We have calculated the partition function of the model and derived the finite-temperature behavior of different physical quantities: namely, the chemical potential, the compressibility, the local magnetic moment, and the specific heat. We have discussed the changes of such observables across the point of the metal-insulator transition  $U=2t$ , providing explicit low-temperature expressions for  $C_V$  and  $\mu$ ; in particular  $\mu$  is found to undergo an unusual transition from a linear to a  $T \ln T$  dependence. We have then focused on the specific heat, which turns out to exhibit interesting features, such as a

nearly universal crossing point and a double-peak structure. The two peaks, which are shown to be related to charge degrees of freedom only, are present in ranges of  $U/t$  both below and above the metal-insulator transition value. We have discussed the two peaks in terms of the kinetic and potential contributions to the spectrum, outlining the differences between the cases of strong coupling and moderate coupling, and comparing our results with that of the ordinary Hubbard model.

The method presented here to derive the partition function of our model can be applied, with straightforward generalization, to further integrable extended Hubbard models<sup>26</sup> involving two Sutherland species. Work is in progress along these lines.

\*Electronic address: fdolcini@athena.polito.it

<sup>†</sup>Electronic address: montorsi@athena.polito.it

<sup>1</sup>F. Dolcini and A. Montorsi, Phys. Rev. B **63**, R121103 (2001).

<sup>2</sup>J. Hubbard, Proc. R. Soc. London, Ser. A **276**, 238 (1963).

<sup>3</sup>F. Gebhard, *The Mott Metal-Insulator Transition: Models and Methods* (Springer-Verlag, Berlin, 1997).

<sup>4</sup>V.J. Emery, Phys. Rev. Lett. **58**, 2794 (1987); F. C. Zhang and T.M. Rice, Phys. Rev. B **37**, 3759 (1988); D.K. Campbell, J.T. Gammel, and E.Y. Loh, Jr. *ibid.* **42**, 475 (1990).

<sup>5</sup>F.H.L. Essler, V.E. Korepin, and K. Schoutens, Phys. Rev. Lett. **68**, 2960 (1992); **70**, 73 (1993); J. de Boer and A. Schadschneider, Phys. Rev. Lett. **75**, 4298 (1995); R.Z. Bariev, A. Klümper, and J. Zittartz, Europhys. Lett. **32**, 85 (1995); **39**, 441 (1997); I.N. Karnaukhov, Phys. Rev. B **57**, 3863 (1998); **62**, 3033 (2000).

<sup>6</sup>L. Arrachea and A.A. Aligia, Phys. Rev. Lett. **73**, 2240 (1994); A. Schadschneider, Phys. Rev. B **51**, 10 386 (1995).

<sup>7</sup>R. Micnas, J. Ranninger, S. Robaszkiewicz, and S. Tabor, Phys. Rev. B **37**, 9410 (1988); R. Micnas and J. Ranninger, S. Robaszkiewicz, *ibid.* **39**, 11 653 (1989).

<sup>8</sup>K.A. Penson and M. Kolb, Phys. Rev. B **33**, 1663 (1986); A. Hui and S. Doniach, *ibid.* **48**, 2063 (1993); S. Robaszkiewicz and B.R. Bulka, *ibid.* **59**, 6430 (1999); F. Dolcini and A. Montorsi, *ibid.* **62**, 2315 (2000).

<sup>9</sup>A.A. Aligia and L. Arrachea, Phys. Rev. B **60**, 15 332 (1999); G.I. Japarize and A.P. Kampf, *ibid.* **59**, 12 822 (1999); K. Maiti, D.D. Sarma, T. Mizokawa, and A. Fujimori, *ibid.* **57**, 1572 (1998); G.S. Jeon, S. Wu, M.Y. Choi, and H.-W. Lee, *ibid.* **59**, 2841 (1999).

<sup>10</sup>M. Takahashi, Prog. Theor. Phys. **52**, 103 (1974).

<sup>11</sup>N. Kawakami, T. Usuki, and A. Okiji, Phys. Lett. A **137**, 287 (1989); T. Usuki, N. Kawakami, and A. Okiji, J. Phys. Soc. Jpn. **59**, 1357 (1990).

<sup>12</sup>G. Jüttner, A. Klümper, and J. Suzuki, Nucl. Phys. B **522**, 328 (1998).

<sup>13</sup>F. Gebhard, A. Girdt, and A.E. Ruckenstein, Phys. Rev. B **49**, 10 926 (1994).

<sup>14</sup>H. Shiba and P.A. Pincus, Phys. Rev. B **5**, 1966 (1972).

<sup>15</sup>R. Schumann, Ann. Phys. (Leipzig) **11**, 49 (2001).

<sup>16</sup>T. Paiva, R.T. Scalettar, C. Huscroft, and A.K. McMahan, Phys. Rev. B **63**, 125116 (2001).

<sup>17</sup>D. Duffy and A. Moreo, Phys. Rev. B **55**, 12 918 (1997).

<sup>18</sup>A. Georges and W. Krauth, Phys. Rev. B **48**, 7167 (1993).

<sup>19</sup>A. Germann and H.V. Löhneysen, Europhys. Lett. **9**, 367 (1989); G.E. Brodale, R.A. Fisher, N.E. Phillips, and J. Flouquet, Phys. Rev. Lett. **56**, 390 (1986).

<sup>20</sup>F. Steglich *et al.*, J. Low Temp. Phys. **95**, 3 (1994).

<sup>21</sup>I. Peschel, X. Wang, M. Kaulke, and K. Hallberg, *Density Matrix Renormalization: A New Numerical Method in Physics* (Springer-Verlag, Berlin, 1999).

<sup>22</sup>A.O. Gogolin, A.A. Nersisyan, and A.M. Tsvelik, *Bosonization Approach to Strongly Correlated Systems* (Cambridge University Press, Cambridge, England, 1999).

<sup>23</sup>M. Gaudin, *La fonction d'onde de Bethe* (Masson, Paris, 1983); N.C. Ha, *Quantum Many Body Systems in One Dimension*, (World Scientific, Singapore, 1996).

<sup>24</sup>V.E. Korepin, N.M. Bogolubov, and A.G. Izergin, *Quantum Inverse Scattering Method and Correlation Functions* (Cambridge University Press, Cambridge, England, 1993).

<sup>25</sup>H.A. Bethe, Z. Phys. **71**, 205 (1931).

<sup>26</sup>F. Dolcini and A. Montorsi, Int. J. Mod. Phys. B **14**, 1719 (2000).

<sup>27</sup>A.J. Bracken *et al.*, J. Phys. A **34**, 4459 (2001).

<sup>28</sup>M. Takahashi, Prog. Theor. Phys. **47**, 69 (1972).

<sup>29</sup>M. Suzuki, Phys. Rev. B **31**, 2957 (1985); M. Suzuki and M. Inoue, Prog. Theor. Phys. **78**, 787 (1987); A. Klümper, Ann. Phys. (Leipzig) **1**, 540 (1992); C. Destri and H.J. de Vega, Phys. Rev. Lett. **69**, 2313 (1992).

<sup>30</sup>G. Jüttner and A. Klümper, Europhys. Lett. **37**, 335 (1997); G. Jüttner, A. Klümper, and J. Suzuki, Nucl. Phys. B **487**, 650 (1997).

<sup>31</sup>G. Jüttner, A. Klümper, and J. Suzuki, J. Phys. A **30**, 1881 (1997).

<sup>32</sup>In fact, it can easily be checked that the Hamiltonian of the  $U = \infty$  Hubbard model can be rewritten as  $\mathcal{P}H_t$ , where  $\mathcal{P}$  rules out double occupancy.

<sup>33</sup>As to the value of  $Y$ , we observe that the models with  $Y > 0$  can be mapped into those with  $Y < 0$  through a mere redefinition of the phase of the doubly occupied state, i.e.,  $|\downarrow\uparrow\rangle_j \rightarrow (-1)^j |\downarrow\uparrow\rangle_j$ ,  $j = 1, \dots, L$ . Therefore, the investigation of the range  $Y \leq 0$  is completely general.

<sup>34</sup>Notice that, with respect to Ref. 1, here it is sufficient to deal only with the off-diagonal part  $\hat{T}_{i,j}$  of the full generalized permutator  $\Pi_{i,j}$  introduced there.

<sup>35</sup>D. Vollhardt, Phys. Rev. Lett. **78**, 1307 (1997).